RAMReS Sciences des Structures et de la Matière Vol. 10, N°1 (2026) 34 - 52
http://publication.lecames.org/index.php/mat *ISSN: 2630-1180*

Cocoa pod-derived biochar for Ibuprofen and Diclofenac adsorption: a low-cost and reusable adsorbent

Mouafo Mouafo F. Joel[1,2,5,6,*], Esaie Kouadio A. Kouassi[2], Abega Aimé Victoire[3], Affoué Tindo S. Konan[4], Briton Henri[2,5], Soro Doudjo[2], Daouda Mama[1,5,6], Yao Kouassi Benjamin[2,5]

[1]*Laboratory of Applied Hydrology (LHA) at the University of Abomey-Calavi in Benin*
[2]*Laboratory of Industrial Process Synthesis, Environmental and New Energy (LAPISIEN) at the Institut National Polytechnique Félix Houphouët-Boigny, Yamoussoukro, Côte d'Ivoire*
[3]*Department of Chemistry, Faculty of Sciences, University of Douala, Douala P.O. Box 24157, Cameroon*
[4]*Laboratory of Thermodynamics and Physico-Chemistry of the Environment (LTPCM), Training and Research Center, Faculty of Fundamental and Applied Science (UFR-SFA), Nangui Abrogoua University, Abidjan, Cote d'Ivoire*
[5]*African Center of Excellence for Water and Sanitation (C2EA)*
[6]*National Institute of Water at University of Abomey-Calavi in Benin (INE)*

Received: 9 December 2025 / Received in revised form: 21 February 2026 / Accepted: 21 April 2026

***Abstract*:**

This study investigates the adsorption potential of biochar derived from cocoa pod husks, both in its raw form and after nitric acid-functionalization, for the removal of two common pharmaceutical pollutants, diclofenac and ibuprofen, from aqueous solutions. The biochars were characterized using BET, XRD, SEM, FTIR, and TGA-DTG techniques. Acid modification significantly enhanced the surface area (235.50 m^2 g^{-1} vs. 213.77 m^2 g^{-1}), thereby increasing the availability of active sites for adsorption. Morphological analysis revealed irregular, porous structures favorable for pollutant trapping. Adsorption kinetics followed a pseudo-second-order model, suggesting chemisorption as the dominant mechanism, while isotherm modelling indicated a combination of physical and chemical interactions, suggesting multi-mode adsorption. Maximum adsorption occurred under highly acidic conditions (pH = 1 for diclofenac, pH = 2 for ibuprofen). Notably, the biochar recovered 63% of its capacity in the first reuse cycle, though performance declined progressively to 39% by the third cycle. These findings position cocoa pod biochar as a cost-effective, sustainable, and reusable adsorbent for pharmaceutical-contaminated water, offering a high-value application for agricultural waste in water purification systems. This research underscores the value of transforming agricultural waste into innovative adsorbents that can help address pollution challenges in wastewater management on a practical scale.

***Keywords* :** Cocoa pods biochar ; Pharmaceutical pollutants ; Adsorption kinetics ; Water treatment ; Biochar regeneration.

* Corresponding author:
Email address: *mouafofranckjoel@yahoo.fr (F.J.M. Mouafo)*
https://doi.org/10.70974/mat10126034

This work is licensed under a Creative Commons Attribution 4.0 International License.

1. Introduction

The ubiquitous presence of pharmaceutical residues in wastewater treatment plant (WWTP) effluents has emerged as a critical environmental challenge, exacerbated by rapid global industrialization and demographic expansion. Given their inherent persistence, high bioactivity, and potential for deleterious ecotoxicological impacts, these compounds are now classified as contaminants of emerging concern (CECs) within aquatic ecosystems [1]. Conventional secondary treatment processes often prove inadequate or economically unfeasible for the complete mineralization of these recalcitrant micropollutants.

Among the most prevalent CECs are non-steroidal anti-inflammatory drugs (NSAIDs), specifically diclofenac [2-(2,6-dichlorophenylamino)phenylacetic acid] (DCF) and ibuprofen [2-(4-isobutylphenyl)propanoic acid] (IBU). Due to their extensive clinical and over-the-counter consumption, DCF and IBU are frequently quantified in surface waters, groundwater, and treated effluents. Diclofenac, widely prescribed for inflammatory and rheumatic disorders, is particularly notorious for its poor biodegradability and high environmental stability. Indeed, DCF frequently bypasses standard wastewater treatment infrastructure, with removal efficiencies often stagnating below 20% [2–4].

Ibuprofen, one of the most prescribed and over-the-counter analgesics globally, is similarly found at concentrations ranging from nanograms to several micrograms per litre (10 to 30 ng L^{-1} up to 1.2 µg L^{-1}) in various water bodies [5–8]. These residues can cause endocrine disruption, behavioural alterations in aquatic organisms, and the potential development of antibiotic resistance [9]. Therefore, finding a solution to this issue is of great importance.

Several technologies have been developed to remove such micropollutants, including chemical precipitation, ion exchange, advanced oxidation processes, membrane filtration, electrochemical methods, biological treatments, and adsorption [3, 10–12]. However, these approaches often suffer from high operational costs, energy demands, or limited effectiveness at trace contaminant levels. Adsorption, on the other hand, has emerged as a competitive alternative due to its operational simplicity, cost-effectiveness, and scalability. Activated carbon remains the benchmark adsorbent but is expensive and energy-intensive to produce, leading researchers to explore bio-based alternatives [6, 13, 14].

Biochar, a carbon-rich porous material derived from the pyrolysis of biomass, has gained increasing attention for environmental remediation due to its high surface area, surface functional groups, and tunable properties [13]. Surface modification, particularly via acid or base activation, is a well-established strategy to enhance adsorption performance by increasing porosity and introducing functional groups (e.g., –COOH, –OH) that can interact with pollutants [11]. Nevertheless, most reported biochars are derived from wood, agricultural residues like rice husks and corn stalks, or even algae, while less attention has been given to cocoa pod husks, despite their global abundance.

Côte d'Ivoire is the world's largest cocoa producer, contributing approximately 42% of global supply with an estimated 2.74 million tons in 2023 [15]. Cocoa pods, which account for about 80% of the harvested fruit mass, are largely discarded post-harvest and remain underutilized, posing environmental disposal challenges for smallholder farmers. Transforming this biomass waste into functional biochar offers a dual advantage: reducing the agricultural residue burden and creating value-added products for environmental protection.

In this study, we investigate the adsorption potential of biochar derived from cocoa pod husks, both untreated and nitric acid-functionalized, for the removal of diclofenac and ibuprofen from aqueous media. The materials were characterized by Brunauer–Emmett–Teller (BET) surface area analysis, scanning electron microscopy (SEM), X-ray diffraction (XRD), Fourier-transform infrared spectroscopy (FTIR), and thermogravimetric analysis (TGA-DTG). Adsorption kinetics, isotherms, and thermodynamic parameters were analysed to elucidate the mechanisms involved. Additionally, regeneration experiments were conducted to evaluate the reusability and sustainability of the adsorbents. The results highlight the potential of functionalized cocoa pod biochar as an efficient, low-cost, and sustainable solution for removing pharmaceutical contaminants from water systems.

2. Experimental

2.1. Materials

Sodium diclofenac ($C_{14}H_{10}Cl_2NNaO_2$, ≥ 98%), ibuprofen ($C_{13}H_{18}O_2$, ≥ 98%), sodium carbonate (Na_2CO_3, 98%), sodium bicarbonate ($NaHCO_3$, 98%), absolute ethanol (C_2H_6O), sodium chloride (NaCl, > 99%), hydrochloric acid (HCl, 37%), and sodium hydroxide (NaOH, >98%) were purchased from Sigma-Aldrich (St. Louis, MO, USA). Sodium thiosulfate pentahydrate ($Na_2S_2O_3{\cdot}5H_2O$), potassium iodide (KI, 99%), iodine (I_2, 99.9%), and methanol (CH_3OH) were supplied by Chem-lab (Zedelgem, Belgium). Nitric acid (HNO_3, 69%) was obtained from Sisco Research Laboratories (Mumbai, India). All chemicals were used as received without further purification.

2.2. Methods

2.2.1. Preparation of Biochar and Functionalized Biochar

Raw cocoa pods were collected from rural plantations near Yamoussoukro, Côte d'Ivoire. The biomass underwent a multi-step cleaning process involving tap water and deionized water rinses, followed by manual fragmentation and a two-week sun-drying period. To ensure complete moisture removal, the material was further dried at 105 °C for 24 h in a laboratory oven, subsequently crushed, and sieved to a particle size ≤ 2.5 mm. Pyrolysis was conducted by placing 30 g of the prepared biomass in a ceramic crucible within a muffle furnace (LHT 02/17 LB, Nabertherm GmbH, Germany). Carbonization was performed at 300, 400,

and 500 °C for 1 h, maintaining a constant heating rate of 10 °C min^{-1}. The resulting biochars were screened based on their iodine and methylene blue adsorption capacities to identify the optimal precursor for chemical activation.

Surface functionalization was achieved by refluxing 100 g of the selected biochar with 250 mL of 5 mol L^{-1} HNO_3 at 80 °C for 5 h. The oxidized mixture was then cooled, washed repeatedly with deionized water until a neutral pH was reached, and finally dried at 105 °C for 24 h to obtain the functionalized adsorbent.

2.2.2. Adsorption experiments

Stock solutions of diclofenac (40 mg L^{-1}) and ibuprofen (30 mg L^{-1}) were prepared by dissolving appropriate amounts in distilled water, followed by 24 h of stirring. Working solutions (1 to 10 mg L^{-1}) were obtained by serial dilution. The absorbance of the solutions was measured using a UV-Visible spectrophotometer (UV-1800, Shimadzu, Kyoto, Japan) at 267 nm (diclofenac) and 262 nm (ibuprofen).

Adsorption experiments were conducted by adding 0.05 g of biochar or functionalized biochar to 30 mL of pharmaceutical solution in Erlenmeyer flasks. After agitation at room temperature for predetermined times, the mixtures were filtered, and the equilibrium concentration was measured. The amount adsorbed (Q_e, mg g^{-1}) and removal percentage (R, %) were calculated using Equations (1) and (2), respectively.

$$Q_e = \frac{(C_0 - C_t)V}{m_{\mathrm{ACP}}} \tag{1}$$

$$R = \frac{(C_0 - C_t)}{C_0} \times 100 \tag{2}$$

where C_0 is the initial concentration of the adsorbate (mg L^{-1}), C_t is the equilibrium concentration of the adsorbate (mg L^{-1}), V is the volume of the solution containing the adsorbate (mL), m is the mass of the adsorbent (g), and R is the removal rate. The initial pH and the initial concentration of the adsorbate in solution are the parameters that have been varied to optimize adsorption. The initial pH of the solutions was adjusted using hydrochloric acid and sodium hydroxide solutions of normality 0.1 mol L^{-1}.

2.2.3. Thermodynamic study

Thermodynamic experiments were performed using solutions with concentrations ranging from 30 to 70 mg L^{-1}. A 0.02 g mass of adsorbent was added to 30 mL of solution and agitated for 20 minutes at temperatures of 15, 20, 30, 40, and 50 °C. The filtrates were analysed by UV-Visible spectrophotometry. The data were used to calculate the standard Gibbs free energy ($\Delta G°$), enthalpy ($\Delta H°$), and entropy ($\Delta S°$) changes.

2.2.4. Material characterization

Textural properties, including specific surface area (SSA) for both raw and functionalized biochars, were characterized via N_2 adsorption-desorption isotherms at 77 K using a V-Sorb 2800S analyzer (Gold APP Instruments). The SSA was quantified through the multipoint Brunauer-Emmett-Teller (BET) model [16]. Concurrently, pore volume and average pore diameter were derived from the adsorption branch of the isotherms using the Barrett-Joyner-Halenda (BJH) method. Scanning electron microscopy (SEM) analysis, performed using a HIROX SH-4000 M spectrophotometer, was conducted to investigate the surface morphology of the biochar and the functionalized biochar. Additionally, energy-dispersive X-ray spectroscopy (EDS) analysis was utilized to determine the elemental composition and map the distribution of elements within the activated material.

Fourier-transform infrared spectroscopy was performed to determine the functional groups present on the biochar and functionalized biochar surfaces in the range of 400 to 4000 cm^{-1}. The method used was the KBr pellet technique.

X-ray diffraction (XRD) was employed to investigate the internal structure of the materials. XRD analysis was conducted using a Siemens X-ray diffractometer at the NGRL LABORATORY in Nigeria.

Thermogravimetric analysis (TGA) was performed to monitor mass changes in the samples as a function of temperature. The analysis was carried out using a PerkinElmer thermogravimetric analyzer equipped with differential thermal analysis (DTA) capabilities. Experimental conditions included a heating rate of 10 °C min^{-1}, a sample mass of approximately 17 mg, and a maximum temperature of 950 °C.

2.2.5. Boehm titration

The surface acidity and basicity of the prepared materials were evaluated by Boehm titration. Functional groups on the carbon surface were quantified by titrating 0.1 g samples with 0.1 mol L^{-1} solutions of NaOH, HCl, Na_2CO_3, and $NaHCO_3$ for 72 h. The resulting solutions were back-titrated to determine phenolic, lactonic, carboxylic, and basic functional groups.

2.2.6. Zero-point charge pH (pH_{pzc})

The pH_{pzc} defines the pH at which the total surface charge of a material is zero. Determining the pH_{pzc} of the biochar and functionalized biochar consists of preparing a NaCl solution of concentration 0.1 mol L^{-1} at pH ranging between 2 and 10 by adding NaOH or HCl. A volume of 40 mL of each solution was introduced into an Erlenmeyer flask containing 0.1 g of adsorbent. The determination of this point makes it possible to predict possible interactions between the molecules of the adsorbent and those of the adsorbate after plotting $pH_i = f(\Delta pH)$.

2.2.7. Regeneration studies

To assess reusability, 10 mg of exhausted adsorbent was treated with 20 mL of 0.1 mol L^{-1} HCl, NaOH, methanol, or distilled water for 1 h. The samples were then washed, dried at 80 °C, and reused under identical adsorption conditions (0.02 g adsorbent, 20 mL solution, 30 min). Adsorption efficiency was compared across cycles.

3. Results and discussion

3.1. Biochar physicochemical properties

3.1.1. Thermogravimetric analysis

The pyrolysis of cocoa pod husks, conducted between 300 and 500 °C based on TGA profiles, resulted in a progressive yield reduction from 47% to 40%. This downward trend is primarily attributed to the thermal degradation of hemicellulose, cellulose, and lignin. This decomposition triggers the loss of structural water and volatile organic matter, alongside the evolution of syngas components such as CH_4, CO, H_2, and CO_2 at elevated temperatures [4, 17]. Process optimization identified 300 °C as the favourable carbonization temperature, yielding a product with balanced properties: a mass yield of 47%, an iodine value of 567.69 mg g^{-1}, and a methylene blue adsorption capacity of 82.02 mg g^{-1}. The thermogravimetric (TGA), differential scanning calorimetry (DSC), and derivative thermogravimetric (DTG) curves of the cocoa pod raw material in the temperature range of 30 to 700 °C under an inert atmosphere and a heating rate of 10 °C min^{-1} are presented in figure 1. From this figure, we observe four mass losses: the first one (7.93%) at 77 °C relates to the departure of water molecules adsorbed on the precursor surface. The second and main mass loss (53.46%) observed between 273 and 295 °C can be attributed to the decomposition of hemicellulose, which was the main constituent of the precursor. At 404 °C, we have a mass loss of 16.42% corresponding to the decomposition of cellulose, and the last one at 442 °C with a mass loss of 5.72% was attributed to the decomposition of lignin [17, 18].

3.1.2. Textural characteristics (BET, ash content, humidity percentage)

The biochar BET specific surface area provides an indication of its adsorption capacity. The BET surface area, a key indicator of adsorption capacity, was significantly higher for the functionalized biochar (235.50 m^2 g^{-1}) compared to the reference biochar (213.765 m^2 g^{-1}). Nitric acid treatment enhanced the surface area by increasing pore volume and introducing acidic functional groups, improving interactions with polar molecules. Nitric acid attack increased the specific surface area by creating new micropores or widening existing ones. The BJH average pore diameter of 2.1 nm (Table 1) indicates that HNO_3 functionalization shifts the biochar structure to the micropore-mesopore transition threshold. This evolution is attributed to oxidative etching, where nitric acid widens existing micropores into narrow mesopores. This hybrid porosity is advantageous, as it maintains a high surface area while reducing mass-transfer resistance for large molecules like diclofenac. The biochar and nitric acid-functionalized biochar prepared from cocoa pods in this study exhibited a higher or comparable specific surface area to those reported in the literature, such as medium-density fiberboard residues (2.3 m^2 g^{-1}) [19], banana (4.7 m^2 g^{-1}), cassava (13.2 m^2 g^{-1}), pig manure (3.4–63 m^2 g^{-1}) [20], rice husk (63–76 m^2 g^{-1}) [21], and industrial Kraft lignin (111 m^2 g^{-1}) [22]. According to the European Biochar Certificate (EBC) standard, the specific surface area of biochar must be greater than 150 m^2 g^{-1} [23]. These results exceed the EBC standard (150 m^2 g^{-1}), demonstrating the potential of these cocoa pod-derived biochars for adsorption applications. According to ASTM D2867, a good quality coal should have a moisture content of less than 5%; however, the literature presents coals with moisture content higher than this value that exhibit good adsorption capacity [24].

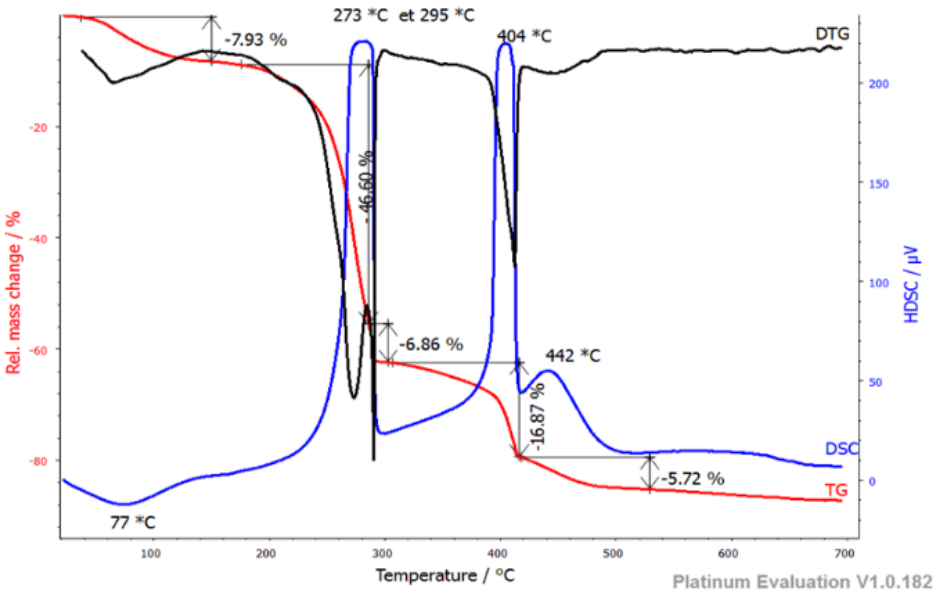

Fig. 1. TGA, DSC, DTG analysis.

Table 1
Textural characteristics.

Parameter	Biochar	Functionalized biochar
Specific surface area (multipoint BET, $m^2\ g^{-1}$)	213.8	235.5
Pore volume (BJH cumulative adsorption, $cm^3\ g^{-1}$)	0.1288	0.1321
Pore diameter (BJH cumulative adsorption, nm)	2.138	2.128
Ash content (%)	15	13
Moisture content (%)	5	5
pH_{pzc}	6.5	4.3

3.1.3. Morphological features

The SEM images of biochar and functionalized biochar are shown in figure 2.

Figure 2 displays images of the morphology of biochar and functionalized biochar at two particle sizes (100 and 20 µm) and two magnifications (500× and 3000×). Both biochar and functionalized biochar exhibit significant structural heterogeneity. Scanning electron microscopy (SEM) reveals that all samples possess a random and irregular structure. The particles are characterized by sharp edges and rough surfaces, with a wide range of sizes. They also demonstrate a high degree of porosity, consistent with the results of BET analysis. The surface morphology is highly irregular and rough, featuring a porous, flaky structure typical of lignocellulosic materials. The surface is marked by large, uneven cracks, voids, and granular debris, all contributing to increased roughness and a larger available surface area for adsorption, as reported in the literature.

Nitric acid functionalization has induced slight morphological modifications, characterized by the appearance of larger pores within the biochar. Both samples show notable porosity, resulting from the pyrolysis-induced degradation of lignin and cellulose within the biochar structure [24]. Nitric acid creates surface roughness and cavities. This increase in roughness and porosity translates into an increase in the specific surface area of the functionalized material. Thus, the treated biochar offers more active sites for molecule adsorption, improving the retention capacities. We observe the formation of new structures, such as aggregates or mineral salt deposits, on the material's surface (white colour). The surface appears rougher and more irregular, indicating the successful introduction of functional groups. BET results show an increase in specific surface area, thus confirming an increase in the adsorption capacity of the functionalized biochar.

3.1.4. Zero charge point pH (pH_{pzc})

The BC and functionalized BC used in this study exhibited a pH below 7 (Table 1 and figure 3), suggesting a predominance of acidic functional groups on their surfaces. This acidic surface favours the adsorption of anions and is consistent with the general principle that below the zero-point charge, carbon surfaces are positively charged and favour anionic adsorption [14, 25].

3.1.5. Boehm titration

Surface functional groups of biochar are identified and quantified using Boehm titration. Acidic oxygen groups are distinguished based on their acid strengths. Boehm titration results showed a high abundance of acidic functional groups compared to basic ones. In contrast, nitric acid-functionalized biochar exhibits an acidic character owing to the predominance of basic functional groups over acidic ones. This acidity of the functionalized biochar surface stems from the use of nitric acid as a functionalizing agent [14, 25]. These results are in line with the point of zero charge (pH_{pzc}) value falling within the acidic range (Figure 4).

The Boehm titration results support the FTIR findings of reduced intensity for certain oxygen-containing groups.

3.1.6. FTIR analysis

The distribution of surface functional groups for the cocoa pods and derived biochars is presented in figure 5; a general decrease in group intensity is observed across all samples before the adsorption process. FTIR analysis revealed the presence of several functional groups in the precursor. For the raw material, a broad peak between 3500–3000 cm^{-1} suggests the presence of hydroxyl (-OH) groups from oxygenated functional groups, or even absorbed water. The hydroxyl (-OH) group acts as a primary donor/acceptor for hydrogen bonding with the carboxyl and amine groups of the pharmaceutical molecules. The presence of aliphatic C-H stretching (near 2900 cm^{-1}) points to hydrophobic regions on the biochar matrix that attract the non-polar moieties of the adsorbates.

Additionally, the weak peaks around 2500–2300 cm^{-1} indicate the presence of methylene groups or the stretching vibration of C≡C bonds around 2200 cm^{-1}. Peaks at 1650 and 1300 cm^{-1} indicate the presence of aromatic groups (Reddy et al., 2011). These peaks confirm the graphitic nature of the biochar, which facilitates strong π-π stacking interactions with the aromatic rings of both diclofenac and ibuprofen. This structural feature facilitates strong π-π stacking interactions between the sp^2-hybridized carbon layers of the biochar and the aromatic rings of both diclofenac and ibuprofen.

The peak at 1056 cm^{-1} corresponds to the C-O stretching vibrations of alcohols and phenols. At 815 cm^{-1}, we have the aromatic C-H bending [3, 4, 12, 26]. For the biochar and the functionalized biochar, we observe a dihydroxylation group due to the increase in temperature, resulting in the breaking of the O-H bond and the loss of hydrogen. Furthermore, Fourier-transform infrared spectroscopy (FTIR) analysis reveals that carbonization and nitric acid functionalization

have caused a deconstruction of the organic matter, manifested by a simplification of the FTIR spectrum (decrease in peak intensities, disappearance of the peak at 1056 cm^{-1} characteristic of the C-O stretching of alcohols and phenols) [4].

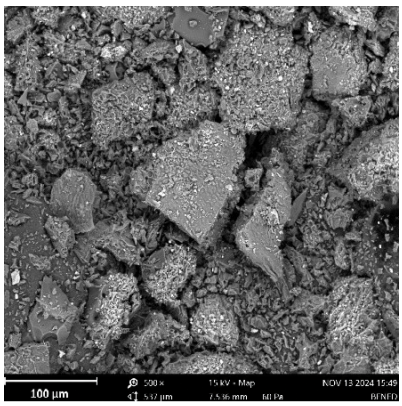

(a)

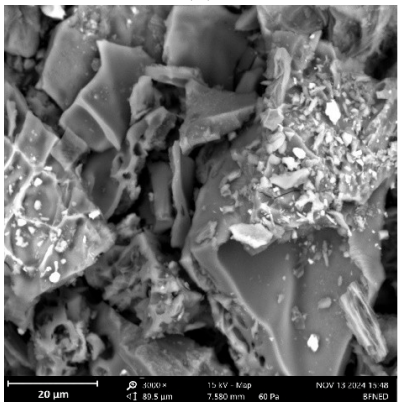

(b)

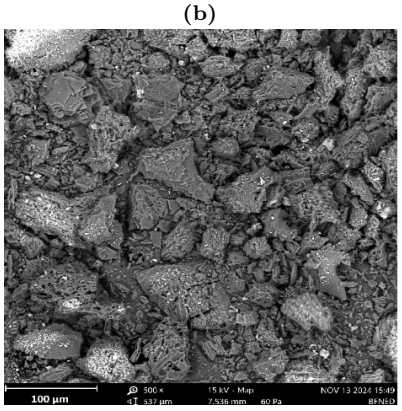

(c)

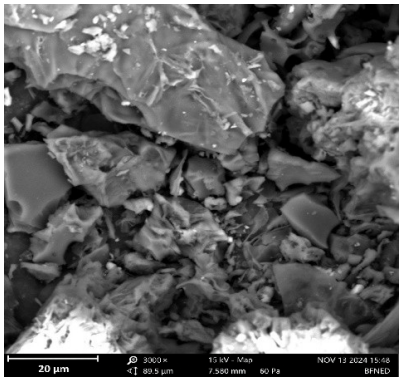

(d)

Fig. 2. SEM images of the biochar (a, b) and the functionalized biochar (c, d).

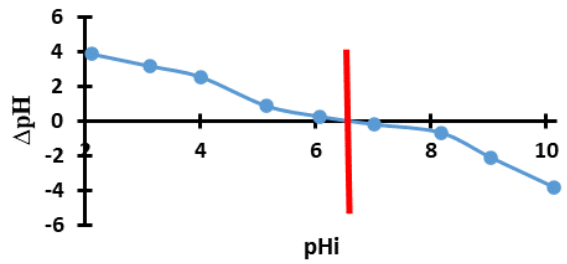

(a)

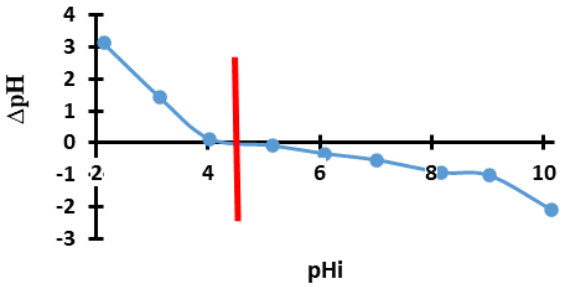

(b)

Fig. 3. pH_{pzc} of biochar (a) and functionalized biochar (b).

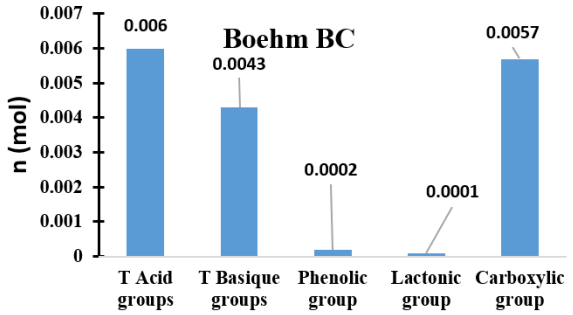

(a)

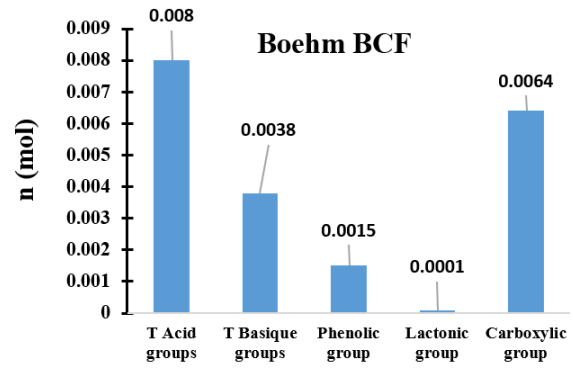

(b)

Fig. 4. Boehm titration of biochar (a) and functionalized biochar (b).

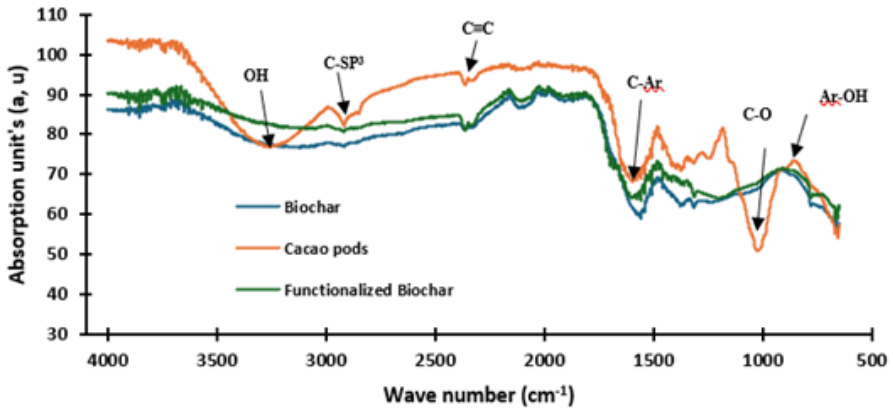

Fig. 5. FTIR of cocoa pods, biochar (BC) and functionalized biochars (BCF) before adsorption.

3.1.7. Structural characteristics (XRD)

X-ray diffraction (XRD) analysis was employed to evaluate changes in the crystallinity of biochars. Figure 6 shows the absence of sharp reflections, indicating the amorphous nature of the prepared biochar and functionalized biochar.

Figure 6 shows a broad band (halo) observed between 20° and 30° centred at 25°, attributed to the (002) Bragg reflections [27]. This is associated with the parallel and azimuthal alignment of the aromatic and carbonized structures, a characteristic of amorphous materials. It indicates the presence of graphite crystallites within the activated carbon (AC) structure. This halo is even more intense for the functionalized biochar, suggesting an increased proportion of the amorphous phase. Concurrently, weak peaks emerge at $2\theta = 25°$, 39°, and 44° for the functionalized biochar, attributable to cristobalite (a mineral composed of silica with the formula SiO_2 and containing traces of Fe, Ca, Al, K, Na, Ti, Mn, Mg, and P). The peak at 44° on the diffractogram of the functionalized biochar, which is attributed to the (100) diffractions of graphitic and hexagonal carbons, reflects the size of the aromatic layer [28]. These results confirm the predominantly amorphous nature of the studied materials, with slight crystallization of cristobalite in the case of the functionalized biochar. The presence of graphene structures, evidenced by the diagrams, is common in biochars derived from the pyrolysis of organic matter.

3.2. Adsorption studies

3.2.1. Influence of pH

The adsorption capacity of biochars for various compounds is significantly influenced by pH. This is because pH alters the charge of the surface functional groups on the biochar, potentially affecting the ionization state of targeted pollutants. The amphoteric nature of biochar allows it to change its surface charge depending on the solution's pH. This behaviour is strongly influenced by the biochar's zero-point charge (pH_{pzc}). The pK_a of the adsorbate (diclofenac: ∼4.15; ibuprofen: ∼4.91) provides insights into the underlying mechanisms of the adsorption process [29]. Indeed, as the pH of the solution increases, the number of negatively charged sites increases. The results display good adsorption capacity at low pH. This result is attributed to the increase in Coulombic interactions between adsorbate molecules (which are negatively charged) and adsorbent particles, which are positively charged at low pH [30]. While the thermodynamic optimum is observed at pH = 1–2, the biochar maintains a robust performance at neutral pH, thereby ensuring its practical applicability for real-world water treatment scenarios. The adsorption performance of both pristine and functionalized biochars was investigated across a pH range of 5.0 to 8.0 to simulate environmentally relevant aquatic conditions. As illustrated in figure 7, the removal efficiencies at pH = 5.0 reached 35% for ibuprofen and 25% for diclofenac, whereas at neutral pH (7.0), these values shifted to 30% and 21%, respectively. The marginal decline in adsorption capacity observed as the alkalinity increased toward pH = 8.0 is primarily attributed to the electrostatic repulsion between the predominantly negative surface charge of the biochar and the anionic forms of the pollutants (pK_a of diclofenac is ≈4.1). Despite this trend, the substantial removal rates maintained at neutral pH underscore the material's practical viability for decentralized wastewater treatment in rural areas, as it bypasses the logistical and financial constraints of chemical pH pre-adjustment. Similar results were obtained by De Luna *et al.* [31] during the adsorption of DCF from cocoa husk-derived chars and by Bernardo *et al.* [32] during their studies on the removal of DCF by activated carbon from potato peels. These results showed that adsorption is favoured in acidic solutions. Similar results were also obtained in a study on the removal of diclofenac by adsorption using activated carbon prepared from olive pomace [4, 33].

3.2.2. Influence of time

Figure 8 presents the influence of time during the adsorption process. Based on this figure, it has been observed that the amount of pollutant removed increases with time until reaching equilibrium at 10 minutes. This curve suggests that the adsorption process occurs in two phases. The increasing adsorption rate observed during the first 5 minutes is attributed to the availability of free adsorption sites for pollutant molecule retention [4, 34, 35].

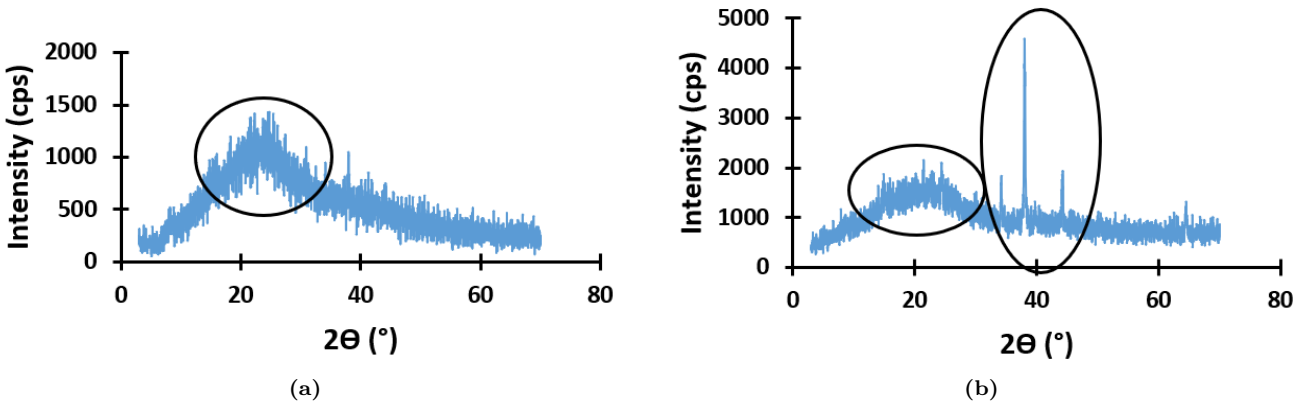

Fig. 6. XRD of biochar (a) and functionalized biochar (b).

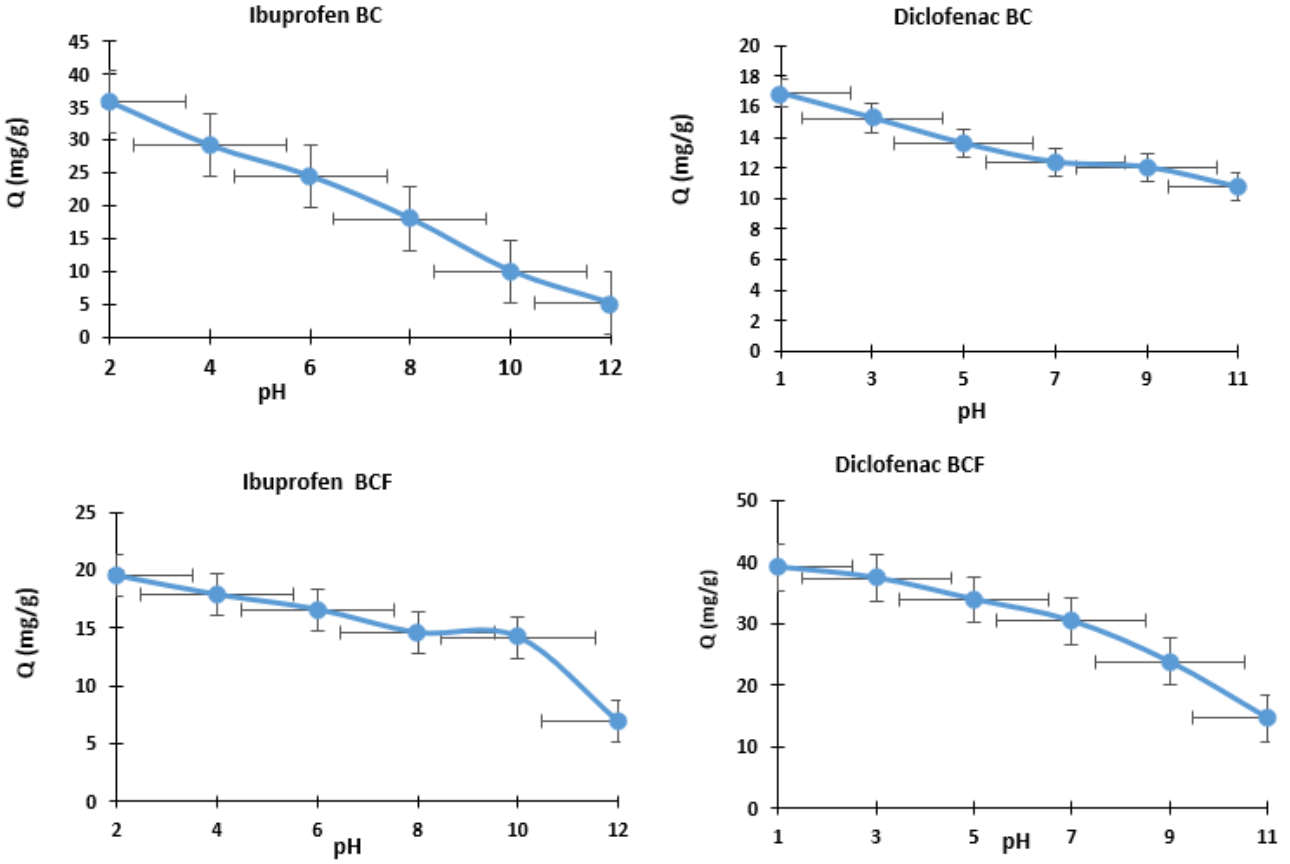

Fig. 7. Influence of pH on the adsorption of ibuprofen and diclofenac by biochar (BC) and functionalized biochar (BCF). Data points represent the mean of triplicate experiments ($n = 3$), with error bars indicating the standard deviation (SD).

The physicochemical affinity between the adsorbate and the biochar matrix facilitates the formation of molecular complexes, thereby promoting the sequestration of chemical species onto the adsorbent's porous framework. This mass transfer process continues until a thermodynamic equilibrium is established, at which point the rate of molecular attachment aligns with the rate of desorption. Experimental data indicates that the system reaches a steady-state distribution between the solid and liquid phases within a 10-minute contact period, suggesting rapid saturation of the primary surface-active sites. Beyond 10 minutes, a plateau is formed, which is explained by the saturation of the solid surface due to the total occupation of the active adsorption sites [25, 36].

3.2.3. *Influence of adsorbent mass*

To evaluate the effect of adsorbent dosage on diclofenac and ibuprofen uptake, the mass was varied from 0.02 to 0.06 g. Experiments were conducted over a 10-minute contact time using initial concentrations of 30 mg L^{-1} (at pH = 1.0) and 40 mg L^{-1} (at pH = 2.0), respectively.

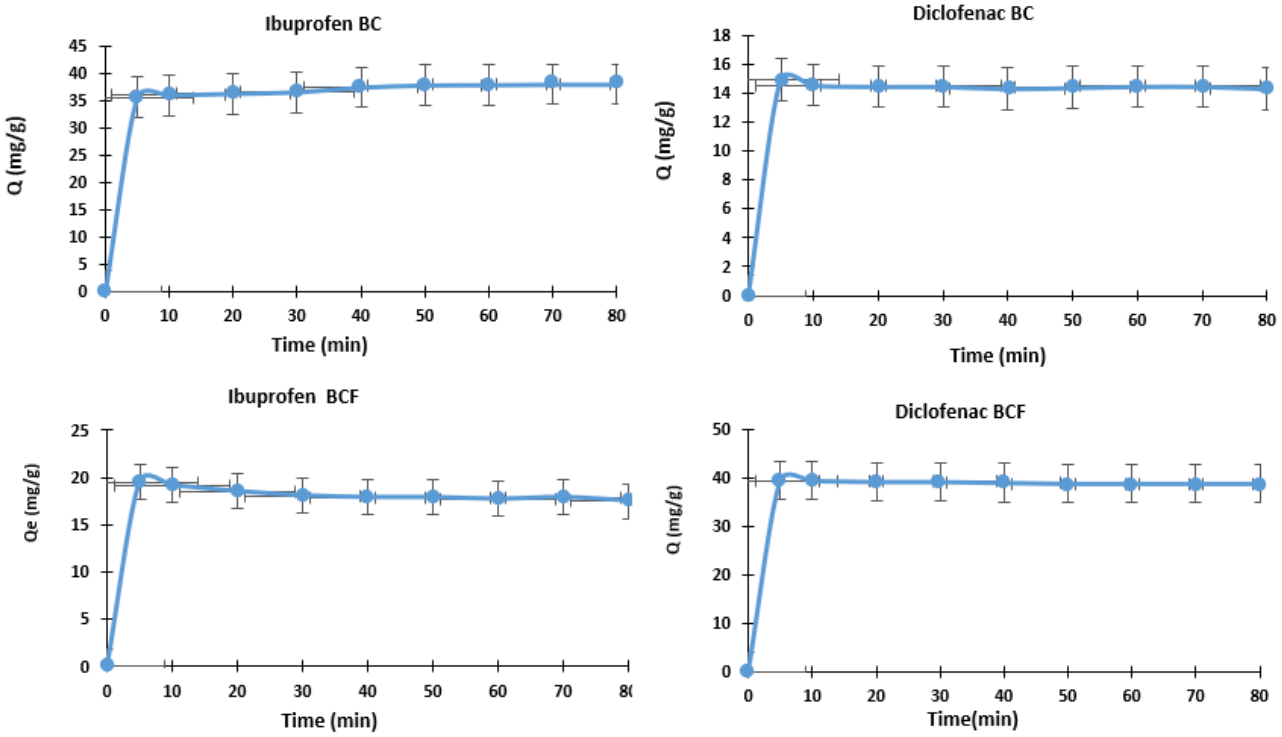

Fig. 8. Influence of time on the adsorption of ibuprofen and diclofenac by biochar (BC) and functionalized biochar (BCF). Data points represent the mean of triplicate experiments ($n = 3$), with error bars indicating the standard deviation (SD).

As shown in figure 9, the adsorption profiles exhibited similar trends for both pollutants. Based on this plot, it can be observed that the amounts of diclofenac and ibuprofen adsorbed decrease with increasing adsorbent mass. This reduced adsorption capacity was attributed to the fact that larger masses lead to an increase in electrostatic interactions between adsorbent molecules, which can cause the desorption of pollutant molecules from the narrow sites of the adsorbent. There was agglomeration of adsorbent particles (aggregate formation). This agglomeration results in a decrease in the contact surface area (due to the overlapping of active biochar sites) and an increase in the diffusion path of the ions to the active sites. With large biochar masses, the cation exchange capacity available in solution is insufficient to cover all the vacant sites present on the adsorbent surface, leading to a lower adsorption capacity for large masses [4, 12, 37]. This reduced adsorption capacity could also be related to the fact that the solution concentration remains fixed and unchanged during the experiment, while the adsorbed quantity is inversely proportional to the mass of the adsorbent [38, 39]. Similar results have been obtained by Lekene *et al.* [4], Ankoro *et al.* [12], and De Luna *et al.* [31].

3.2.4. Influence of initial concentration

It has been demonstrated that the adsorbate concentration is a crucial factor and needs to be considered as it has an impact on the mass transfer of molecules to the adsorbent surface [40]. The influence of initial concentration was studied by varying the concentration of diclofenac and ibuprofen from 30 to 100 mg L^{-1} for 10 minutes with 0.02 g of biochar at pH = 1 and 2 for diclofenac and ibuprofen, respectively (Figure 10). The results demonstrate that adsorption increases with increasing adsorbate concentration. This behaviour is attributed to the fact that the adsorption capacity is directly proportional to the initial concentration. Furthermore, the observed increase can be explained by a higher concentration gradient, which acts as a driving force to overcome mass transfer resistance. This reduced resistance, coupled with a decrease in the mean free path between adsorbate molecules, promotes more frequent collisions with the adsorbent surface. Consequently, a larger number of ions migrate toward the available active sites, leading to enhanced pollutant retention. The increase could also be attributed to the limited availability of additional adsorption sites (a higher number of pollutant molecules in solution per mass of biochar) [41, 42].

To further evaluate how the previously discussed surface properties and pore structures influence the removal capacity, the equilibrium behaviour was investigated through adsorption isotherm studies.

3.2.5. Adsorption isotherm studies

Adsorption isotherms are crucial for determining the maximum adsorption capacity and identifying the type of adsorption that will occur. They are obtained by graphically representing $q_e = f(C_e)$, where q_e and C_e are the equilibrium adsorption amount per gram of BC used and the residual concentration, respectively. To ensure maximum statistical rigour and avoid the inherent biases of linearization, all adsorption isotherm parameters for the biochar were calculated via nonlinear regression analysis.

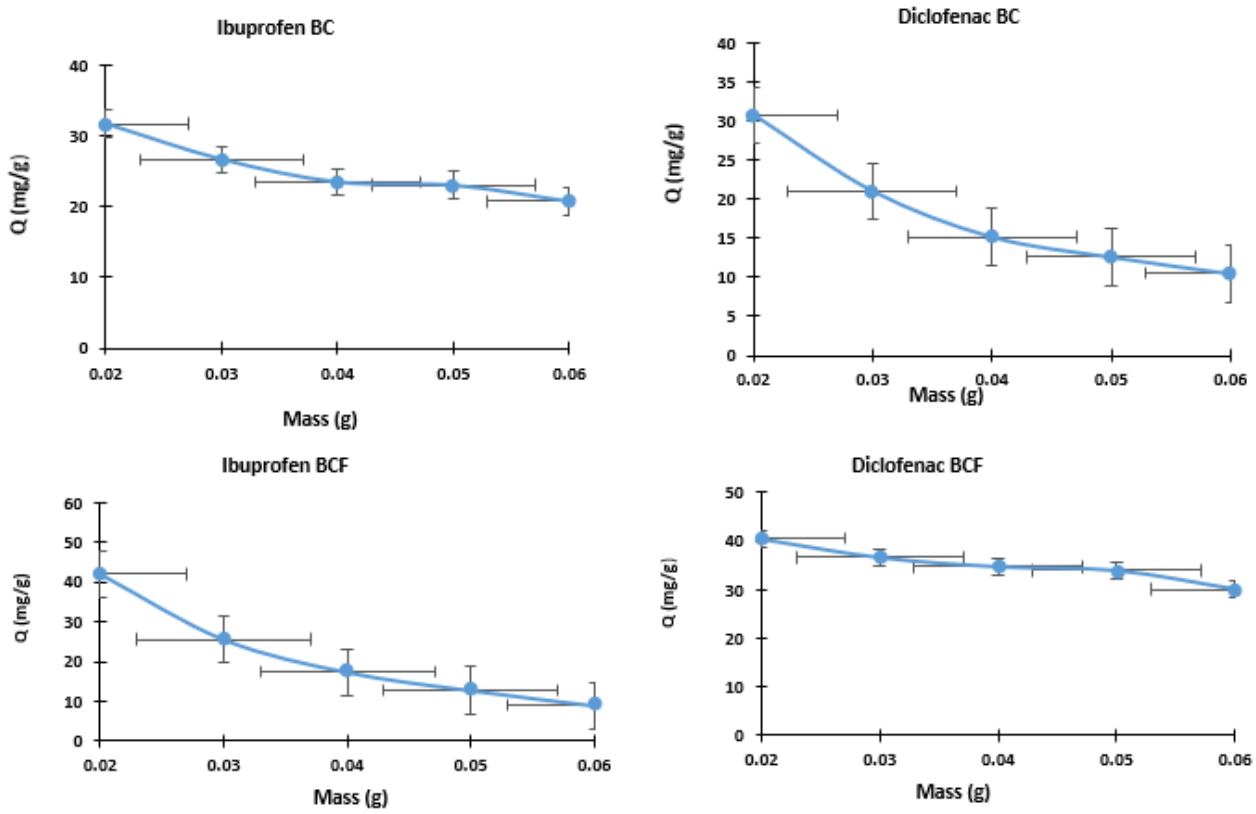

Fig. 9. Influence of mass on the adsorption of ibuprofen and diclofenac by biochar and functionalized biochar. Data points represent the mean of triplicate experiments ($n = 3$), with error bars indicating the standard deviation (SD).

The fitting process was executed by minimizing the objective function through the Solver. Regarding the statistical indicators, while the R^2 values demonstrate a strong correlation, the recorded root mean square error (RMSE) values provide a more realistic measure of the fit quality. Nonlinear transformations of some isotherm models are represented in figure 11 below and were all found to be H-type according to the Giles classification [43]. It can be seen that when the initial concentration of adsorbates increased, the amount adsorbed also increased. However, this rise eventually plateaued due to a limitation in available adsorption sites on the adsorbent. This competition between adsorbate molecules for the remaining sites suggests a monolayer adsorption process. The observed behaviour aligns with weak intermolecular forces, like van der Waals forces, governing the adsorption of ibuprofen and diclofenac [43].

In the present work, to describe the adsorption mechanism, two models with two parameters (Langmuir and Freundlich) were chosen (Table 2).

For the biochar, based on the results obtained, the Langmuir constant (K_L) values are less than 1, indicating favourable adsorption for both adsorbates [4].

The Langmuir model assumes that all binding sites possess identical energy and are equally accessible, which aligns with the observed plateau in q_e at higher C_e concentrations. Considering the obtained RMSE and χ^2 values, the Langmuir model provides a better fit for ibuprofen adsorption with R^2 coefficients of 0.99 and 0.99 for BC and BCF, respectively, while the Freundlich model better describes diclofenac adsorption with R^2 values of 0.99 and 0.96 for diclofenac by BC and BCF, respectively. This is further supported by the high R^2 values, close to 1 for both models, indicating a strong correlation between the experimental data and the fitted models.

These findings suggest that ibuprofen adsorption on both BC and BCF follows the Langmuir isotherm, implying monolayer adsorption onto a homogeneous surface. In contrast, the better fit of the Freundlich isotherm for diclofenac adsorption suggests a multilayer adsorption mechanism onto a heterogeneous surface for both adsorbents.

For the Freundlich isotherm, $1/n$ values are less than 1, indicating favourable adsorption for both adsorbents [4, 43]. Since K_L is less than 1, we can conclude that adsorption is favourable for both adsorbates [44]. Given the relatively low RMSE and χ^2 values and the high R^2 value, we observe monolayer adsorption on a homogeneous surface for ibuprofen adsorption and multilayer adsorption on a heterogeneous surface for diclofenac adsorption [45].

3.3. Adsorption kinetics studies

Adsorption kinetics is a crucial aspect in the study of pollutant removal [40] (Shan et al., 2015). It provides valuable information for understanding adsorption mechanisms [46].

Adsorption kinetics is particularly important as it allows for the determination of adsorption efficiency by assessing the pollutant removal rate and the time

required to reach equilibrium. Additionally, it helps in predicting the rate-limiting steps of the process [12].

Four models were selected to evaluate this aspect: pseudo-first-order, pseudo-second-order, Elovich, and intra-particle diffusion models.

Based on the R^2, RMSE, and χ^2 values, both pseudo-first-order (R^2: 0.996–0.999; RMSE: 0.175–0.72; χ^2: 0.016–0.15) and pseudo-second-order models (R^2: 0.985–0.999; RMSE: 0.24–0.63; χ^2: 0.023–0.25) effectively describe the elimination kinetics of ibuprofen and diclofenac for biochar and functionalized biochar (see Table 3 for complete data). The close agreement between experimental and predicted adsorption values suggests that these models well describe the adsorption mechanism [4, 47].

The removal mechanism likely involves a combination of physisorption and chemisorption due to the good fit of both models. Additionally, the significantly higher adsorption constants (α) compared to desorption constants (β) confirm a chemisorption mechanism on a heterogeneous surface. The non-zero intercept ($C > 0$) implies that intra-particle diffusion is not the only rate-controlling step. The initial resistance to mass transfer indicates that film diffusion (boundary layer diffusion) also contributes significantly to the overall adsorption kinetics. Table 3 presents the different results.

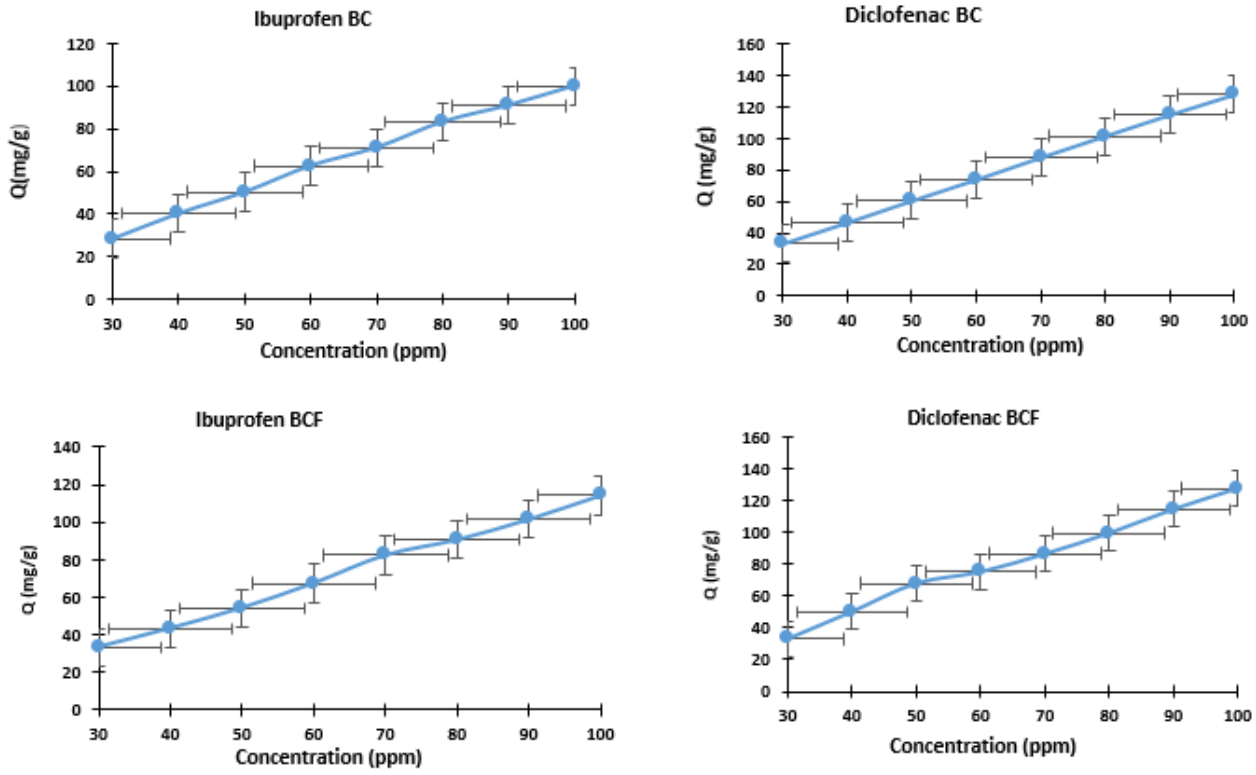

Fig. 10. Influence of concentration on the adsorption of ibuprofen and diclofenac by biochar (BC) and functionalized biochar (BCF). Data points represent the mean of triplicate experiments ($n = 3$), with error bars indicating the standard deviation (SD).

Table 2
Langmuir and Freundlich isotherm adsorption parameters for the adsorption of ibuprofen and diclofenac by biochar and functionalized biochar.

Model	Parameter	Biochar		Functionalized biochar	
		Ibu	Dicl	Ibu	Dicl
Langmuir	R^2	0.99	0.99	0.99	0.91
	Q_m (mg g^{-1}, theoretical)	138.31	273.24	137.18	193.37
	K_L (L mg^{-1})	0.0042	0.61	0.0046	0.068
	RMSE	4.55	21.03	1.89	42.39
Freundlich	R^2	0.98	0.99	0.96	0.96
	K_F (mg g^{-1} (L mg^{-1})$^{-1/n}$)	1.70	0.19	5.15	5.25
	$1/n$	1.2	2.22	0.96	0.98
	RMSE	3.11	2.04	5.12	5.17
	χ^2	2.12	28.07	1.70	1.85

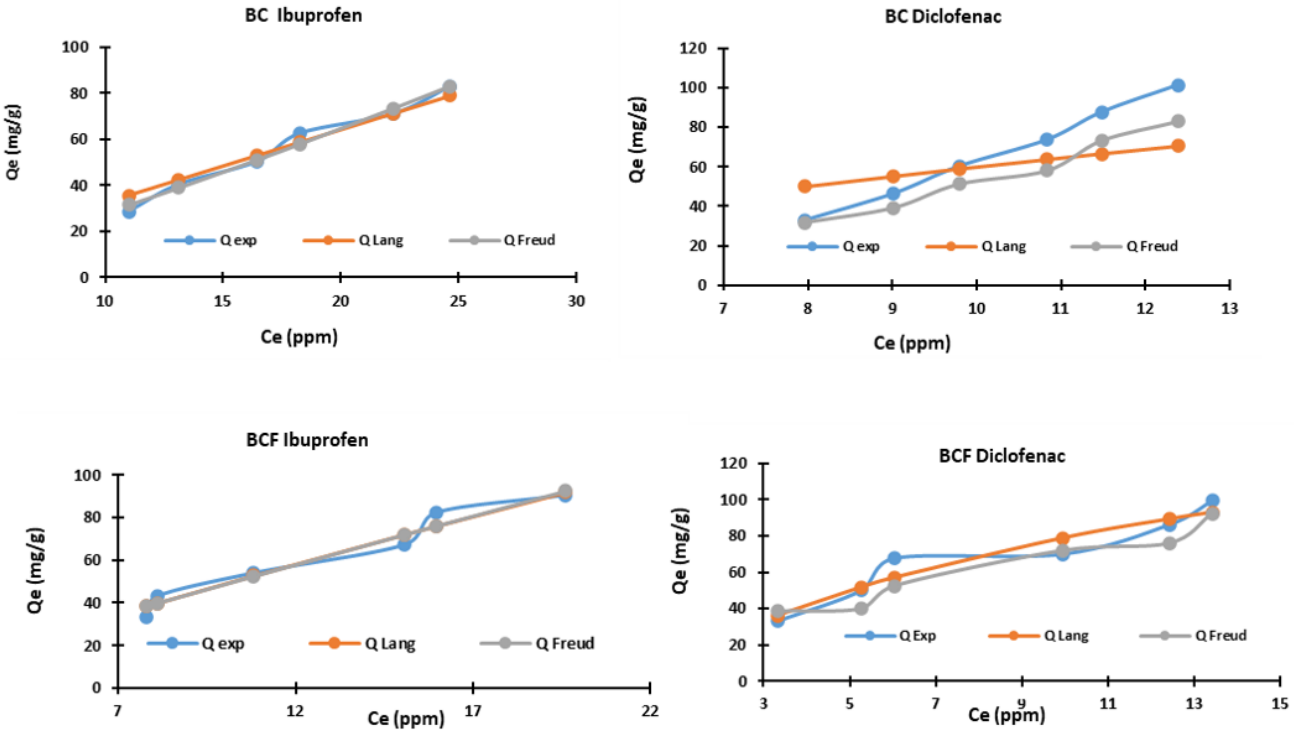

Fig. 11. Isotherm models (Langmuir and Freundlich) of BC and BCF for diclofenac and ibuprofen.

3.4. FTIR after adsorption

Figure 12 shows the FTIR spectra of the biochar and functionalized biochar after adsorption of diclofenac and ibuprofen, respectively. It can be observed that the spectra of the biochar before adsorption and that of ibuprofen after adsorption are almost identical, which suggests a physisorption process, and different for functionalized biochar in which new absorption bands appeared (chemisorption). Regarding the IR spectra of the biochar before and after adsorption of diclofenac, an increase in the intensity of all peaks and the appearance of new peaks, particularly between 1200–1000 cm^{-1}, is observed.

3.5. Adsorption thermodynamics studies

To assess the temperature effect on ibuprofen and diclofenac removal, five temperatures and five concentrations were tested. Data were collected for each adsorbent and adsorbate. Standard adsorption enthalpy (ΔH°), standard entropy (ΔS°), and Gibbs free energy (ΔG°) were calculated using equations to describe the thermodynamic behaviour of adsorption for various adsorbates. Table 4 summarizes these parameters.

Analysis of the enthalpy (ΔH°) values obtained in the table reveals positive values for almost all materials except for the adsorption of ibuprofen onto functionalized biochar. These positive values indicate an endothermic process during the adsorption of ibuprofen and diclofenac [4, 48]. The negative value observed for the adsorption of ibuprofen onto functionalized biochar suggests an exothermic process, illustrating an energetically stable process.

It is important to note that the enthalpy values for all cases, including biochar with ibuprofen and diclofenac (14.24 and 14.31 kJ mol^{-1}), functionalized biochar with diclofenac (13.77 kJ mol^{-1}), and functionalized biochar with ibuprofen (−10.41 kJ mol^{-1}), are lower than 80 kJ mol^{-1}. This observation confirms the involvement of physisorption in the adsorption mechanism of the different adsorbates [4, 49]. Analysis of the standard entropy (ΔS°) values reveals positive values for all materials. This observation indicates an increase in the disorder of diclofenac and ibuprofen molecules at the solid-liquid interface [4, 49]. This increase in entropy can be attributed to the increased degree of freedom of diclofenac and ibuprofen molecules at the surface of the adsorbent material. This also suggests an increase in the randomness of interactions between the adsorbent and adsorbate molecules during the adsorption process. The positive nature of the entropy values also corroborates the endothermic nature of adsorption [50]. However, entropy values decrease with increasing BC functionalization. This could be due to the increase in surface functional groups, which enhances adsorbent-adsorbate interaction by minimizing the translational disorder of the pollutant molecules. The thermodynamic behaviour of the adsorption process was evaluated through the Gibbs free energy change (ΔG°). The negative values of ΔG° calculated for all adsorbents confirm the spontaneity and thermodynamic feasibility of the pharmaceutical uptake. Furthermore, the trend of increasingly negative ΔG° values with rising temperature [4, 48, 49, 51] indicates that the adsorption process becomes more favourable at higher temperatures. This enhancement in spontaneity suggests an endothermic nature of the interaction, likely due to the increased mobility of the adsorbate molecules and the enlargement of the adsorbent pore structure at elevated temperatures.

Table 3
Pseudo-first-order, pseudo-second-order, Elovich, and intraparticle kinetic fitting parameters for ibuprofen and diclofenac onto biochar and functionalized biochar.

Model	Parameter	Biochar		Functionalized biochar	
		Ibu	Dicl	Ibu	Dicl
Pseudo-first-order	Q_e (pred) (mg g^{-1})	37.50	14.44	18.16	39.02
	k_1 (min^{-1})	0.581	3.36	4.986	3.44
	R^2	0.996	0.998	0.987	0.999
	RMSE	0.72	0.175	0.58	0.24
	χ^2	0.15	0.023	0.20	0.016
Pseudo-second-order	Q_e (pred) (mg g^{-1})	37.929	14.44	18.45	39.019
	k_2 (min^{-1})	0.065	5.90	34	98.51
	R^2	0.998	0.996	0.985	0.999
	RMSE	0.458	0.184	0.63	0.24
	χ^2	0.062	0.025	0.25	0.016
Elovich	α (mg g^{-1} min^{-1})	1.39×10^{12}	7.8×10^{32}	2.38×10^{21}	6.40×10^{17}
	β (g min^{-1})	0.844	5.628	4.53	1.51
	R^2	0.998	0.993	0.956	0.990
	RMSE	0.36	0.336	1.086	1.078
	χ^2	0.039	0.087	0.76	0.33
Intra-particle diffusion	k_{id}	2.12	0.710	0.81	0.71
	C_i (mg g^{-1})	20.73	8.75	11.49	8.74
	R^2	0.76	0.61	0.49	0.61
	RMSE	8.14	3.43	4.51	3.43
	χ^2	10.13	4.61	6.375	4.61

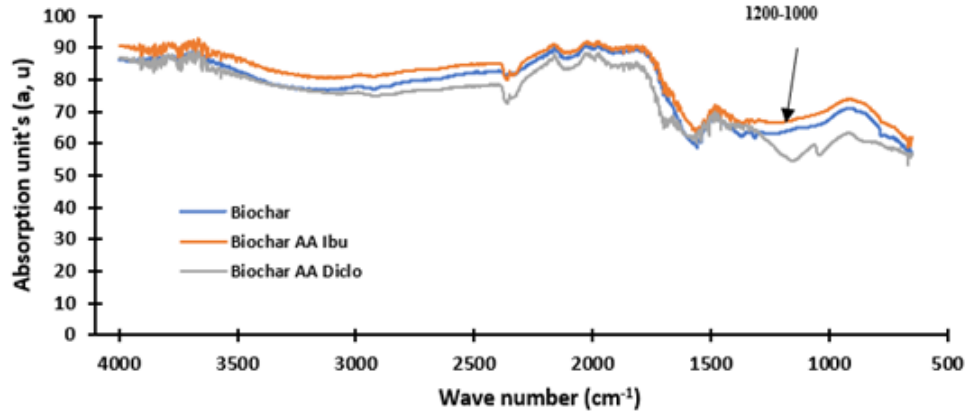

(a)

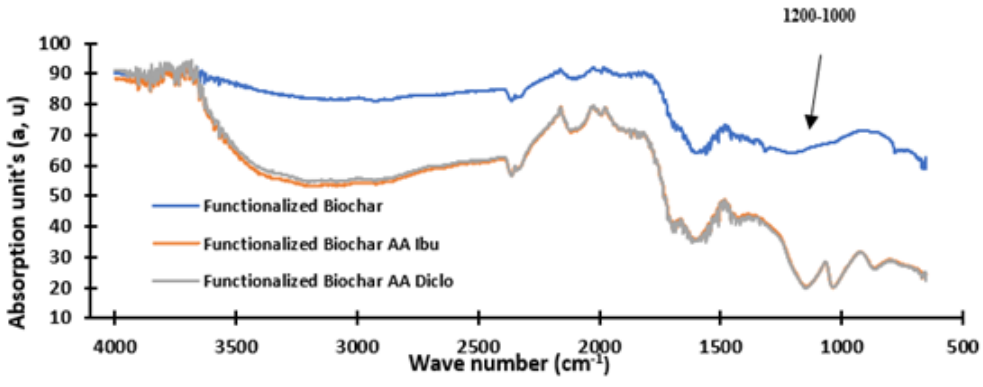

(b)

Fig. 12. FTIR after adsorption of biochar (a) and functionalized biochars (b) for diclofenac and ibuprofen

Table 4
Thermodynamic parameters of the adsorption of ibuprofen and diclofenac onto biochar and functionalized biochar.

Adsorbent	Adsorbate	T (K)	ΔG° (kJ mol^{-1})	ΔH° (kJ mol^{-1})	ΔS° (J mol^{-1} K^{-1})	R^2
Biochar	Ibuprofen	288	−10.416	14.24	85.44	0.72
		293	−10.317			
		303	−12.243			
		313	−12.638			
		323	−13.042			
Biochar	Diclofenac	288	−9.090	14.31	81.04	0.94
		293	−9.331			
		303	−10.185			
		313	−11.344			
		323	−11.706			
Functionalized biochar	Ibuprofen	288	−14.337	−10.41	7.41	0.11
		293	−10.775			
		303	−12.002			
		313	−12.896			
		323	−13.308			
Functionalized biochar	Diclofenac	288	−9.379	13.77	79.93	0.83
		293	−9.273			
		303	−10.720			
		313	−11.461			
		323	−11.827			

In order to evaluate the reusability of the prepared adsorbents, regeneration studies were conducted on biochar and functionalized biochar.

3.6. Regeneration studies

Table 5 presents the results of adsorption tests after regeneration of adsorbents on diclofenac. From these results, it is evident that regeneration using hydrochloric acid yields the best degradation rate for both adsorbents, followed by methanol, distilled water, and finally sodium hydroxide. These results can be attributed to the affinity between the adsorbent surface functional groups and hydronium ions produced from hydrochloric acid. The acidity of the solution allows for the breaking of bonds between the adsorbed molecules and the adsorbent surface functional groups, creating new pores, which could be linked to the strong protonation of the adsorbent surface. Table 5 presents the desorption efficiency.

Table 5
Desorption efficiency of biochar and functionalized biochar using various desorbing agents.

Desorbing agent	Desorption efficiency (%) on diclofenac	
	Biochar	Functionalized Biochar
HCl (0.1 mol L^{-1})	63.54	47.77
Methanol (96%)	60.39	45.92
Distilled water	47.77	43.60
NaOH (0.1 mol L^{-1})	43.60	43.14

This could be due to the presence of oxygen-containing functional groups such as nitro, carboxylic acid, carbonyl, and hydroxyl groups, making the material susceptible to easy desorption and regeneration with an acidic desorption agent [52, 53]. Methanol, a polar solvent with the ability to form hydrogen bonds, is an effective solvent for extracting certain organic molecules adsorbed on the biochar and functionalized biochar surface. As for regeneration with distilled water, it is limited and effective only for water-soluble compounds. To determine the reusability of the prepared biochar and functionalized biochar, the adsorption and regeneration processes were repeated three times. Table 6 presents the obtained results.

Table 6
Desorption efficiency of biochar and functionalized biochar using HCl.

Number of cycles	Desorption efficiency (%) on diclofenac by HCl	
	Biochar	Functionalized Biochar
1	63.54	47.77
2	47.77	37.11
3	39.89	28.76

During the regeneration process, the biochar loses some of its active sites in each cycle owing to the strong chemical bonds due to chemisorption, which negatively impacts the regeneration process [54, 55]. In this study, the results have proven the potential of HNO_3-functionalized biochar adsorbent and cocoa pod biochar as a cost-effective precursor for the sustainable remediation of emerging pharmaceutical pollutants

such as ibuprofen and diclofenac.

4. Cost evaluation and economic-environmental analysis

The cost-effectiveness of large-scale biochar production for wastewater treatment is crucial [4]. This study assessed the production cost of cocoa pod biochar in Côte d'Ivoire, focusing on the energy-intensive drying and pyrolysis stages. Given the relatively low cost of electricity in Côte d'Ivoire (around USD 0.16 kWh^{-1}), the estimated production cost for 1 kg of biochar was determined to be USD 2.56. Further cost reduction could be achieved through sun-drying of the raw material, making biochar a promising, sustainable, and economically viable solution for wastewater treatment. Table 7 presents the cost evaluation.

A comparative analysis with existing literature (Table 8) reveals that the current biochar exhibits significant adsorption potential. Removal efficiency competes with high-cost activated carbons. This performance is largely governed by the presence of oxygen-containing functional groups and the developed microporosity, which facilitate strong π-π interactions and hydrogen bonding with the aromatic rings of the pharmaceutical molecules.

Table 7
Cost evaluation and economic-environmental analysis.

Component	Sub-section	Cost breakdown	Total cost (USD)
Raw material processing	Collection of raw materials for BC production	Cocoa pods were collected from a local market for free	0.00
Preparation of BC	Pyrolysis process	Hours × power × cost per unit = 1 × 1.5 × 0.16	0.24
	Functionalization	Hours × power × cost per unit = 5 × 0.5 × 0.16	0.40
	Drying process	Hours × power × cost per unit = 24 × 0.5 × 0.16	1.92
Washing	Washing process	Deionized water used for washing was obtained from a laboratory set-up	0.00
		Total	2.56

Table 8
Comparison of adsorption capacities with literature.

Adsorbent	Preparation method	Q_{max} (mg g^{-1})	pH, T (°C) concentration (mg L^{-1})	Pollutant	Reference
Cocoa pod AC	Wet impregnation with phosphoric acid	46.95	6.4, 30, 1000	Fe(II)	[56]
Cocoa pod AC	Acid activation	37.49	4, 26, 60	2,4-Dichlorophenol	[57]
Cocoa pod AC	Alkaline-acid activation	100	6, 50, 40	Methylene blue	[58]
Cocoa pod AC	Acid activation	12	6, 80, 0.84	Methylene blue	[59]
Cocoa pod biochar	Mild HNO_3 reflux functionalization	127.48	1, 25, 30	Diclofenac	Present study
Cocoa pod biochar	Mild HNO_3 reflux functionalization	114.39	2, 25, 30	Ibuprofen	Present study

5. Conclusion

Cocoa husk biochar was investigated for its potential to remove diclofenac and ibuprofen from wastewater. The biochar and the functionalized biochar were characterized to determine their surface properties, pore structure, and adsorption capacity. Batch adsorption experiments revealed that both biochars effectively removed the pollutants, with maximum adsorption capacities of 127.71–127.48 mg g^{-1} for diclofenac and 99.86–114.23 mg g^{-1} for ibuprofen on biochar and functionalized biochar, respectively. Most importantly, our optimized cocoa husk biochar exhibits a superior adsorption capacity and faster kinetics compared to several benchmark adsorbents reported in recent literature, such as raw agricultural residues and commercially available activated carbons. The optimal pH for adsorption was 1 for diclofenac and 2 for ibuprofen. Pseudo-second-order kinetic models best described the adsorption process, indicating monolayer chemisorption on an energetically heterogeneous surface. Langmuir and Freundlich isotherm models were well-suited for representing the adsorption mechanism, suggesting a combination of physisorption and chemisorption. FTIR analysis confirmed the adsorption mechanism: physisorption for biochar and chemisorption for the functionalized biochar. Thermodynamic parameters indicated an endothermic and spontaneous process under

favourable conditions. The regeneration study showed that HCl was the best regeneration agent, and after four regeneration cycles, it was observed that the material remains reusable. BET results showed an increase in specific surface area after functionalization (from 213.8 to 235.5 m^2 g^{-1}), thus confirming an increase in the adsorption capacity of the functionalized biochar. X-ray diffraction revealed that the diffractogram of biochar has no significant peaks, characteristic of an amorphous material. Characterization of the functionalized biochar confirms a predominantly amorphous structure, with minor crystalline phases attributed to cristobalite. SEM micrographs reveal significant structural heterogeneity in both raw and functionalized biochars; however, the nitric acid treatment effectively enhanced the surface porosity of the functionalized material. From an economic perspective, the estimated production cost was determined to be USD 2.56 per kg. These findings suggest that cocoa husk biochar, particularly after functionalization optimization, represents a highly sustainable and cost-effective adsorbent for large-scale wastewater remediation.

Data availability

The dataset generated and analysed during this study can be obtained from the corresponding author upon reasonable request.

Funding

World Bank; French Development Agency; Benin Republic; Center of Excellence in Africa for Water and Sanitation Ph.D. program.

Acknowledgments

This work was financially supported by the World Bank, the French Development Agency, the Benin Republic through the Center of Excellence in Africa for Water and Sanitation Ph.D. program. The authors thank Abdourahamane Adamou Ibro for transporting our materials for the XRD, BET, and SEM analyses. The authors of this manuscript sincerely thank the entire research team of the National Institute of Water at the University of Abomey-Calavi in Benin, the Applied Hydrology Laboratory of the University of Abomey-Calavi in Benin, the Laboratory of Industrial Process Synthesis, Environmental and New Energy (LAPISIEN), and the Fab-Lab chimie at INP-HB at the Institut National Polytechnique Félix Houphouët-Boigny, Yamoussoukro, Côte d'Ivoire.

References

[1] O. El Mountassir, M. Bahir, D. Ouazar, A. Chehbouni, P.M. Carreira, *Temporal and spatial assessment of groundwater contamination with nitrate using nitrate pollution index (NPI), groundwater pollution index (GPI), and GIS (case study: Essaouira basin, Morocco)*, Environ. Sci. Pollut. Res. 17 (2022) 17132–17149. https://doi.org/10.1007/s11356-021-16922-8

[2] A. Naima, F. Ammar, O. Abdelkader, *Development of a novel and efficient biochar produced from pepper stem for effective ibuprofen removal*, Bioresour. Technol. 347 (2022) 126685. https://doi.org/10.1016/j.biortech.2022.126685

[3] P.V. Viotti, W.M. Moreira, O.A. Andreo dos Santos, R. Bergamasco, A.M. Salcedo Vieira, M.F. Vieira, *Diclofenac removal from water by adsorption on Moringa oleifera pods and activated carbon: Mechanism, kinetic and equilibrium study*, J. Clean. Prod. 219 (2019) 809–817. https://doi.org/10.1016/j.jclepro.2019.02.129

[4] R.B.N. Lekene, N.M.T. Matemb, M.N.A. Fetzer, T. Strothmann, N.J. Nsami, C. Janiak, *The efficient removal of ibuprofen, caffeine, and bisphenol A using engineered egusi seed shells biochar: Adsorption kinetics, equilibrium, thermodynamics, and mechanism*, Environ. Sci. Pollut. Res. 37 (2023) 29377. https://doi.org/10.1007/s11356-023-29377-w

[5] D. Veclani, M. Tolazzi, F. Fogolari, A. Melchior, *Mechanism and thermodynamics of adsorption of diclofenac on graphene-based nanomaterials*, J. Environ. Chem. Eng. 10 (2022) 108789. https://doi.org/10.1016/j.jece.2022.108789

[6] J. Lach, A. Szymonik, *Adsorption of diclofenac sodium from aqueous solutions on commercial activated carbons*, Desalin. Water Treat. 186 (2020) 418–429. https://doi.org/10.5004/dwt.2020.25567

[7] N. Genç, E. Durna, E. Erkişi, *Optimization of the adsorption of diclofenac by activated carbon and the acidic regeneration of spent activated carbon*, Water Sci. Technol. 83 (2021) 396–408. https://doi.org/10.2166/wst.2020.586

[8] A. Marchlewicz, U. Guzik, D. Wojcieszynska, *Over-the-counter monocyclic non-steroidal anti-inflammatory drugs in environment–sources, risks, biodegradation*, Water Air Soil Pollut. 226(10) (2015) 355. https://doi.org/10.1007/s11270-015-2622-0

[9] S. Chopra, D. Kumar, *Ibuprofen as an emerging organic contaminant in environment, distribution and remediation*, Heliyon 6 (2020) e04087. https://doi.org/10.1016/j.heliyon.2020.e04087

[10] S.N. Oba, J.O. Ighalo, C.O. Aniagor, C.A. Igwegbe, *Removal of ibuprofen from aqueous media by adsorption: A comprehensive review*, Sci. Total Environ. 780 (2021) 146608. https://doi.org/10.1016/j.scitotenv.2021.146608

[11] B. Czech, M. Kończak, M. Rakowska, P. Oleszczuk, *Engineered biochars from organic wastes for the adsorption of diclofenac, naproxen and triclosan from water systems*, J. Clean. Prod. 288 (2021) 125686. https://doi.org/10.1016/j.jclepro.2020.125686

[12] N.O. Ankoro, D. Kouotou, P.K. Lunga, A.T. Godwin, N.R. Lekene, N.J. Ndi, M.J. Ketcha, *Effect of doping activated carbon based Ricinodendron Heudelotti shells with AgNPs on the adsorption of indigo carmine and its antibacterial properties*, Arab. J. Chem. 13 (2020) 5241–5253. https://doi.org/10.1016/j.arabjc.2020.03.002

[13] D. Huang, G. Zhang, J. Yi, M. Cheng, C. Lai, P. Xu, C. Zhang, Y. Liu, C. Zhou, W. Xue, R. Wang, Z. Li, S. Chen, *Progress and challenges of metal-organic frameworks-based materials for SR-AOPs applications in water treatment*, Chemosphere 263 (2021) 127672. https://doi.org/10.1016/j.chemosphere.2020.127672

[14] A.I. Osman, A. Ayati, M. Farghali, P. Krivoshapkin, B. Tanhaei, H. Karimi-Maleh, M. Sillanpaä, *Advanced adsorbents for ibuprofen removal from aquatic environments: A review*, Environ. Chem. Lett. 22 (2024) 373–418. https://doi.org/10.1007/s10311-023-01647-6

[15] International Cocoa Organization (ICCO), Quarterly Bulletin of Cocoa Statistics, ICCO, November (2023). https://www.icco.org/november-2023-quarterly-bulletin-of-cocoa-statistics

[16] S. Brunauer, P.H. Emmett, E. Teller, *Adsorption of gases in multimolecular layers*, J. Am. Chem. Soc. 60 (1938) 309–319. https://doi.org/10.1021/ja01269a023

[17] P. Veiga, J. da S. Schultz, T.T. Matos et al., *Production of high-performance biochar using a simple and low-cost method: Optimization of pyrolysis parameters and evaluation for water treatment*, J. Anal. Appl. Pyrolysis 148 (2020) 104823. https://doi.org/10.1016/j.jaap.2020.104823

[18] F. Güzel, F. Koyuncu, *Adsorptive removal of diclofenac sodium from aqueous solution via industrial processed citrus solid waste–based activated carbon: optimization, kinetics, equilibrium, thermodynamic, and reusability analyses*, Biomass Conversion and Biorefinery 13 (2023) 2401–2412. https://doi.org/10.1007/s13399-021-01969-x

[19] T.C.F. Silva, L. VergÜtz, A.A. Pacheco, L.F. Melo, N.S. Renato, L.C. Melo, *Characterization and application of magnetic biochar for the removal of phosphorus from water*, An. Acad. Bras. Cienc. 92 (2020) e20190884. https://doi.org/10.1590/0001-3765202020190440

[20] H. Deng, Y.F. Li, S.Q. Tao, A.Y. Li, Q.Y. Li, *Efficient adsorption capability of banana and cassava biochar for malachite green: Removal process and mechanism exploration*, Environ. Eng. Res. 27 (2022) 200530. https://doi.org/10.4491/eer.2020.575

[21] M. Bouzidi, L. Sellaoui, M. Mohamed, D.S. Franco, A. Erto, M. Badawi, *A comprehensive study on paracetamol and ibuprofen adsorption onto biomass-derived activated carbon through experimental and theoretical assessments*, J. Mol. Liq. 376 (2023) 121457. https://doi.org/10.1016/j.molliq.2023.121457

[22] Y. Ngernyen, D. Petsri, K. Sribanthao, K. Kongpennit, P. Pinijnam, R. Pedsakul, A.J. Hunt, *Adsorption of the non-steroidal anti-inflammatory drug (ibuprofen) onto biochar and magnetic biochar prepared from chrysanthemum waste of the beverage industry*, RSC Adv. 13 (2023) 14712–14728. https://doi.org/10.1039/d3ra01949g

[23] A. Sedmihradská, M. Pohořelý, P. Jevič, S. Skoblia, Z. Beňo, J. Farták, B. Čech, M. Hartman, *Pyrolysis of wheat barley straw*, Res. Agric. Eng. 66 (2020) 8–17. https://doi.org/10.17221/26/2019-RAE

[24] N. Rouahna, D.B. Salem, I. Bouchareb, M. Asma, O. Abdel-kader, F. Ammar, H. Noureddine, B. Raj, *Reduction of crystal violet dye from water by pomegranate peel-derived efficient biochar: Influencing factors and adsorption behaviour*, Water Air Soil Pollut. 234 (2023) 5. https://doi.org/10.1007/s11270-023-06338-0

[25] S. Larous, A.H. Meniai, *Adsorption of Diclofenac from aqueous solution using activated carbon prepared from olive stones*, Int. J. Hydrogen Energy 41 (2016) 10380–10390. https://doi.org/10.1016/j.ijhydene.2016.02.150

[26] R.B.N. Lekene, N.O. Ankoro, D. Kouotou, *High-quality low-cost activated carbon/chitosan biocomposite for effective removal of nitrate ions from aqueous solution: Isotherm and kinetics studies*, Biomass Conv. Bioref. 14(17) (2024) 20855-20872. https://doi.org/10.1007/s13399-023-04239-0

[27] O. Samira, Y.S. Lahiouel Salih, B.H. Setti, Y. Leila, A. Samia, *Assessment of PAC's performances for theremoval of amoxicillin and paracetamol in aqueous medium*, PONTE International Journal of Science and Research 76(10/1) (2020) 34-51. https://doi.org/10.21506/j.ponte.2020.10.3

[28] N. Asma, B. Sal. Dhirar, O. Abdelkader, R. Noureddine, B. Omirserik, H-B. Ahmad, *Production of bio-char from Melia azedarach seeds for the crystal violet dye removal from water: Combining of hydro-thermal carbonization and pyrolysis*, Bioengineered 14(1) (2023) 290-306. https://doi.org/10.1080/21655979.2023.2236843

[29] K. Całus-Makowska, A. Grosser, A. Grobelak, H. Białek, E. Siedlecka, *Kinetic study of the simultaneous removal of ibuprofen, carbamazepine, sulfamethoxazole, and diclofenac from water using*

biochar and activated carbon adsorption, and TiO_2 photocatalysis, Desalin. Water Treat. 320 (2024) 100817.
https://doi.org/10.1016/j.dwt.2024.100817

[30] S. Jodeh, F. Abdelwahab, N. Jaradat, I. Warad, S. Larous, A.H. Meniai, *Adsorption of diclofenac from aqueous solution using Cyclamen persicum tubers based activated carbon (CTAC)*, J. Assoc. Arab Univ. Basic Appl. Sci. 20 (2016) 32–38.
http://dx.doi.org/10.1016/j.jaubas.2014.11.002

[31] M.D.G. De Luna, R.R.M. Abarca, C.C. Hua, J.A. Lawas, R.O. Arazo, *Removal of diclofenac sodium from aqueous solutions using cocoa (Theobroma cacao) husk-based activated carbon*, J. Mater. Environ. Sci. 8 (2017) 4052–4064.

https://doi.org/10.1016/j.jece.2017.02.018

[32] M. Bernardo, S. Rodrigues, N. Lapa *et al.*, *High efficacy on diclofenac removal by activated carbon produced from potato peel waste*, Int. J. Environ. Sci. Technol. 13 (2016) 1989–2000.
https://doi.org/10.1007/s13762-016-1030-3

[33] R. Baccar, M. Sarra, J. Bouzid, M. Feki, P. Blanquez, *Removal of pharmaceutical compounds by activated carbon prepared from agricultural by-product*, Chem. Eng. J. 211-212 (2012) 310–317.

[34] A.S. Liyanage, S. Canaday, C.U. Pittman, T. Mlsna, *Rapid remediation of pharmaceuticals from wastewater using magnetic Fe_3O_4/Douglas fir biochar adsorbents*, Chemosphere 258 (2020) 127336.
https://doi.org/10.1016/j.chemosphere.2020.127336

[35] M. Zbair, M. Bottlinger, K. Ainassaari et al., *Hydrothermal carbonization of argan nut shell: Functional mesoporous carbon with excellent performance in the adsorption of bisphenol A and diuron*, Waste Biomass Valor. 11 (2020) 1565–1584.
https://doi.org/10.1007/s12649-018-00554-0

[36] G.Y. AL-Kindi, F.H. AL Ani, N.Kh. Al-Bidri, H.A. Alhaidri, *Diclofenac removal from wastewater by activated carbon*, IOP Conf. Ser.: Earth Environ. Sci. 779 (2021) 012088.
https://doi.org/10.1088/1755-1315/779/1/012091

[37] N.D. Suzaimi, P.S. Goh, N.A.N.N. Malek et al., *Performance of branched polyethyleneimine grafted porous rice husk silica in treating nitrate-rich wastewater via adsorption*, J. Environ. Chem. Eng. 7(4) (2019) 103235.
https://doi.org/10.1016/j.jece.2019.103235

[38] M. González-Hourcade, G. Simões dos Reis, A. Grimm, *Microalgae biomass as a sustainable precursor to produce nitrogen-doped biochar for efficient removal of emerging pollutants from aqueous media*, J. Clean. Prod. 348 (2022) 131288.
https://doi.org/10.1016/j.jclepro.2022.131280

[39] J.B. Njewa, T.T. Biswick, E. Vunain et al., *Synthesis and characterization of activated carbon from agrowastes for the removal of acetic acid from an aqueous solution*, Adsorpt. Sci. Technol. 2022 (2022) 7701128 .
https://doi.org/10.1155/2022/7701128

[40] M. Gayathiri, T. Pulingam, K.T. Lee, K. Sudesh, *Activated carbon from biomass waste precursors: Factors affecting production and adsorption mechanism*, Chemosphere 294 (2022) 133764.
https://doi.org/10.1016/j.chemosphere.2022.133764

[41] M. Antunes, V.I. Esteves, R. Guégan, J.S. Crespo, A.N. Fernandes, M. Giovanela, *Removal of diclofenac sodium from aqueous solution by Isabel grape bagasse*, Chem. Eng. J. 192 (2012) 114–121.
https://doi.org/10.1016/j.cej.2012.03.062

[42] G.V. Nunell, E. Gomez-Delgado, P.R. Bonelli, A.L. Cukierman, *Effectiveness of activated carbons developed by different strategies in the removal of diclofenac sodium and salicylic acid from water*, J. Porous Mater. 29 (2022) 1309–1319.
https://doi.org/10.1007/s10934-022-01252-y

[43] O. Abuzalat, D. Wong, M.A. Elsayed, *Nanoporous composites of activated carbon–metal organic frameworks (Fe-BDC@AC) for rapid removal of Cr(VI): Synthesis, adsorption, mechanism, and kinetics studies*, J. Inorg. Organomet. Polym. Mater. 32 (2022) 1924–1934.
https://doi.org/10.1007/s10904-022-02237-9

[44] V. Gómez-Serrano, M. Adame-Pereira, M. Alexandre-Franco, C. Fernández-González, *Adsorption of bisphenol A by activated carbon developed from PET waste by KOH activation*, Environ. Sci. Pollut. Res. 28 (2021) 24342–24354.
https://doi.org/10.1007/s11356-020-08428-6

[45] P. Nanta, K. Kasemwong, W. Skolpap, *Isotherm and kinetic modeling on superparamagnetic nanoparticles adsorption of polysaccharide*, J. Environ. Chem. Eng. 6 (2018) 794–802.
https://doi.org/10.1016/j.jece.2017.12.063

[46] B. Kocabıyık, O. Üner, Ü. Geçgel, *Diclofenac sodium adsorption in aqueous media by activated carbon obtained from einkorn (Triticum monococcum L.) husk*, Adsorption 30 (2024) 1033–1046.
https://doi.org/10.1007/s10450-024-00479-2

[47] S. Keerthanan, A. Bhatnagar, K. Mahatantila, *Engineered tea-waste biochar for the removal of caffeine, a model compound in pharmaceuticals and personal care products (PPCPs), from aqueous media*, Environ. Technol. Innov. 19 (2020) 100847.
https://doi.org/10.1016/j.eti.2020.100847

[48] A.V. Abega, H.M. Ngomo, I. Nongwe, E.H. Mukaya, P.M.A. Kouoh Sone, X.Y. Mbianda, *Easy and convenient synthesis of CNT/TiO_2 nanohybrid by in-surface oxidation of Ti^{3+} ions and application in the photocatalytic degradation of organic contaminants in water*, Synth. Met. 251 (2019) 1–14.
https://doi.org/10.1016/j.synthmet.2019.03.012

[49] N. Kaya, Z. Yıldız Uzun, C. Altuncan, H. Uzun, *Adsorption of Congo red from aqueous solution onto KOH-activated biochar produced via pyrolysis of pine cone and modeling of the process using artificial neural network*, Biomass Conv. Bioref. 12 (2022) 5293–5315.
https://doi.org/10.1007/s13399-021-01856-5

[50] K. Shahjalal, T. Yusaku, C.S. Ganesh, A. Md Rabiul, K. Takahiro, *Development of synthetic zeolites from bio-slag for cesium adsorption: Kinetic, isotherm and thermodynamic studies*, J. Water Process Eng. 33 (2020) 101036.
https://doi.org/10.1016/j.jwpe.2019.101055

[51] L. Sellaoui, A. Gómez-Avilés, F. Dhaouadi, J. Bedia, A. Bonilla-Petriciolet, S. Rtimi, C. Belver, *Adsorption of emerging pollutants on lignin-based activated carbon: Analysis of adsorption mechanism via characterization, kinetics and equilibrium studies*, Chem. Eng. J. 452 (2023) 139399.
https://doi.org/10.1016/j.cej.2022.139399

[52] J. Bayuo, K.B. Pelig-Ba, M.A. Abukari, *Adsorptive removal of chromium(VI) from aqueous solution unto groundnut shell*, Appl. Water Sci. 9:107 (2019) 1-11.
https://doi.org/10.1007/s13201-019-0987-8

[53] H. Patel, *Review on solvent desorption study from exhausted adsorbent*, J. Saudi Chem. Soc. 25(8) (2021) 101302.
https://doi.org/10.1016/j.jscs.2021.101302

[54] T. Alsawy, E. Rashad, M. El-Qelish, Ramy H. Mohammed, *A comprehensive review on the chemical regeneration of biochar adsorbent for sustainable wastewater treatment*, npj Clean. Water 5:29 (2022) 1-20.
https://doi.org/10.1038/s41545-022-00172-3

[55] H. Tan, R.A. Wahab, P.Y. Ong, P.S. Goh, K. Wong, Y.V. Fan, C.T. Lee, *Chemical regeneration of spent empty fruit bunch biochar for sodium ion adsorption*, Chem. Eng. Trans. 106 (2023) 313-318.
https://doi.org/10.3303/CET23106053

[56] O.A.A. Eletta, F.O. Ayandele, J.O. Ighalo, *Adsorption of Pb(II) and Fe(II) by mesoporous composite activated carbon from Tithonia diversifolia stalk and Theobroma cacao pod*, Biomass Convers. Biorefin. 13 (2023) 9831–9840.
https://doi.org/10.1007/s13399-021-01699-0

[57] S.U. Esidje, J.V. Aimikhe, D. Appah, O.D. Samuel, C.N. Nwaokocha, E.N. Adewuyi, *Development of activated carbon for carbon dioxide capture using cocoa pod waste in the tropic*, Proc. SPIE 13279 (2024) 1327934-1–1327934-11.

[58] Z. Guerra-Que, K.S. López-Margalli, J.M. Urrieta-Saltijeral, A.A. Silahua-Pavón, H. Martínez-García, P. García-Alamilla, J.G. Torres-Torres, *Activated carbon synthesised from lignocellulosic cocoa pod husk via alkaline and acid treatment for methylene blue adsorption: optimisation by response surface methodology, kinetics, and isotherm modelling*, RSC Adv. 15 (2025) 47231–47254.
https://doi.org/10.1039/d5ra05557a

[59] D.L. Kouadio, Y.A.H. Yapi, D.E.J.C. Meledje, K.A.P. Dalogo, D.P.V. Akesse, B. Dibi, K.S. Traore, *Desorption of methylene blue adsorbed on activated carbon from cocoa pod shell*, Open J. Appl. Sci. 13 (2023) 605–617.
https://doi.org/10.4236/ojapps.2023.135048